

The bipolar structure of the LBV nebula around HR Carinae

K. Weis^{1,2*}, W.J. Duschl^{1,3}, D.J. Bomans^{2*,**}, Y.-H. Chu^{2*}, and M.D. Joner^{4*}

¹ Institut für Theoretische Astrophysik, Tiergartenstr. 15, D-69121 Heidelberg, Germany

² University of Illinois, Department of Astronomy, 1002 W. Green Street, Urbana, IL 61801, USA

³ Max-Planck-Institut für Radioastronomie, Auf dem Hügel 69, D-53121 Bonn, Germany

⁴ Brigham Young University, Dept. of Physics and Astronomy, 263 FB, Provo, UT 84602, USA

Received 1 July 1996 / Accepted 12 September 1996

Abstract. HR Carinae is one of the few Luminous Blue Variables (LBVs) in the Galaxy. It has a nebula that appears bipolar. We have obtained imaging and high-dispersion, long-slit echelle data of the HR Car nebula, and confirmed that it is a bipolar nebula. Its polar axis lies along the position angle of $125 \pm 5^\circ$; each lobe has, at a distance of 5 kpc a diameter of ~ 0.65 pc and a line-of-sight expansion velocity of $75 - 150 \text{ km s}^{-1}$.

Beside the expanding bipolar lobes, a number of [N II]-bright knots are detected. These knots have lower expansion velocities than the lobes and are detected only within the projected boundary of the lobes. These knots are most likely nitrogen-enriched material ejected by HR Car.

On a larger scale, a funnel-shaped nebula is detected at $2'5$ northwest of HR Car. The axis of the funnel is roughly aligned with the polar axis of the HR Car nebula, suggesting that HR Car may be responsible for the ionization and shaping of this nebula. Future observations of kinematics and abundances are needed to determine the nature of this nebula.

We propose that the bipolar nebula of HR Car is a more evolved version of the Homunculus Nebula around η Car. The recently developed theory of wind-compressed disks may explain the higher density of the equatorial plane and the formation of bipolar nebulae of LBVs.

Key words: Stars: evolution – Stars: individual: HR Car; η Car – Stars: mass-loss – ISM: bubbles: jets and outflows

Send offprint requests to: K. Weis
email: kweis@ita.uni-heidelberg.de

* Visiting Astronomer, Cerro Tololo Inter-American Observatory, National Optical Astronomy Observatories, operated by the Association of Universities for Research in Astronomy, Inc., under contract with the National Science Foundation.

** Feodor-Lynen Fellow of the Alexander von Humboldt Foundation

1. Introduction

Luminous Blue Variables (LBVs) are often found in small circumstellar nebulae, which contain the mass lost by these evolved supergiants (Nota et al. 1995). With an initial mass $\geq 50 M_\odot$, these stars start as main-sequence O stars and evolve towards cooler temperatures at the end of hydrogen-core burning. Following this track they enter the LBV phase when they approach the Humphreys-Davidson limit (e.g. Langer et al. 1994; García-Segura et al. 1996). The Humphreys-Davidson limit is an empirical upper boundary in the HR diagram (Humphreys & Davidson 1979). Stars near this boundary are very unstable and show the highest mass-loss rates observed, several $\times 10^{-4} M_\odot \text{ yr}^{-1}$. Losing more and more mass via continuous stellar winds and violent outbursts or eruptions, LBVs never reach the red supergiant phase but enter the Wolf-Rayet state after $\simeq 25000 \text{ yr}$ in the LBV phase (Humphreys & Davidson 1994). The copious mass loss associated with the violent eruptions is responsible for the formation of a circumstellar nebula. An excellent example is given by the LBV η Carinae, around which the LBV nebula (LBVN) corresponds to eruptions mainly in 1840 – 1860 (Polcaro and Viotti 1993; Viotti 1995).

The star HR Carinae (also known as HD 90177, SAO 238005, He 3-407) is one of the few LBVs known in our Galaxy. Its spectral type varies from B2I to B9I; strong Balmer, Fe II and [Fe II] emission lines are observed, with the Balmer and Fe II lines showing P Cygni profiles (Carlson & Henize 1979; Hutsemékers & Van Drom 1991). The distance to the star has been derived using two different methods which give consistent results: kinematic distance $r_{\text{kin}} = 5.4 \pm 0.4 \text{ kpc}$ (Hutsemékers & Van Drom 1991), and reddening distance $r_{\text{red}} = 5 \pm 1 \text{ kpc}$ (van Genderen et al. 1991). Therefore, HR Car has a luminosity

of $M_{\text{bol}} = -9^m0 \pm 0^m5$, comparable to the other LBVs. The circumstellar nebula around HR Car was not discovered until 1991, making it one of the newest member of LBVs (Hutsemékers & Van Drom 1991). The origin and shape of the nebula around HR Car has been discussed by Hutsemékers (1994). A high-resolution image and a spectropolarimetric study have been presented by Clampin et al. (1995).

We have obtained deep $H\alpha$ CCD images and high-dispersion, long-slit echelle observations of the nebula around HR Car. The images are used to examine the structure of the circumstellar nebula and large-scale gaseous environment of HR Car. The echelle data are used to study the internal motion of the HR Car nebula. In this paper we report our analysis of the environment, kinematics, age, and evolution of the nebula around the LBV HR Car.

2. Observation and data reduction

2.1. Imaging

Images of the field around HR Car have been taken with a CCD camera on the 0.9m telescope at the Cerro Tololo Inter-American Observatory in March 1996. The seeing was between $1''.4$ and $2''$ during the observations. An $H\alpha$ filter and Strömgren y filter were used. The $H\alpha$ filter, having a central wavelength of 6563 \AA and a filter width of 75 \AA included the $[\text{NII}]$ lines at $\lambda 6548 \text{ \AA}$ and $\lambda 6583 \text{ \AA}$. The Strömgren y filter was used to obtain continuum images to facilitate the continuum subtraction from the $H\alpha$ images. The 2048×2048 Tek2K3 CCD was used, and the pixel size was approximately $0''.4$.

To avoid saturation of the bright star HR Car itself, we secured multiple short exposures. A total of 10 frames in the y filter and 60 frames in the $H\alpha$ filter were taken, each having 30 s exposure. To speed up the readout, only the central 1024×1024 pixels were read, hence the field of view was $6'.75 \times 6'.75$. The combined $H\alpha$ image centered on HR Car is shown in Fig. 1.

A funnel-shaped nebulosity is detected to the northwest of HR Car in Fig. 1. To investigate the spatial extent of this nebulosity, a second set of 5 $H\alpha$ and 5 y frames of 300 s exposure each were taken of the adjacent field. The combined $H\alpha$ image of the second field is displayed in Fig. 2. Note that the faint oval halo, $\sim 2'.5 \times 2'.1$, around HR Car in Fig. 1 is not present in Fig. 2, indicating that this halo is probably caused by the internal scattering inside the telescope optics rather than being real emission.

HR Car, the star itself, is so much brighter than the surrounding nebula that it is necessary to subtract the continuum image from the $H\alpha$ image to obtain a better view of the nebula. We have subtracted the scaled, combined y image from the combined $H\alpha$ image. The scaling factor is estimated using the neighboring stars. HR Car is a strong $H\alpha$ emitter and hence cannot be removed completely in the continuum-subtracted $H\alpha$ image. The cen-

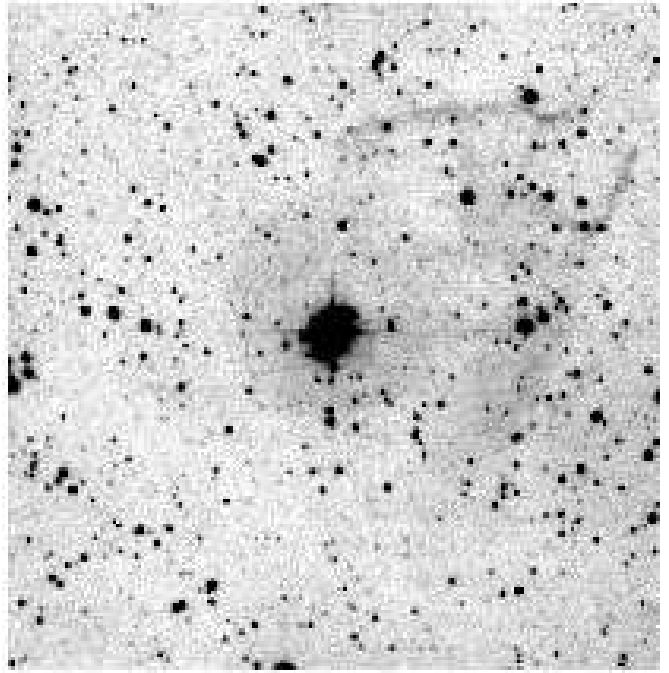


Fig. 1. $H\alpha$ image centered on HR Car. The field of view is $6'.75 \times 6'.75$. North is up and east is to the left.

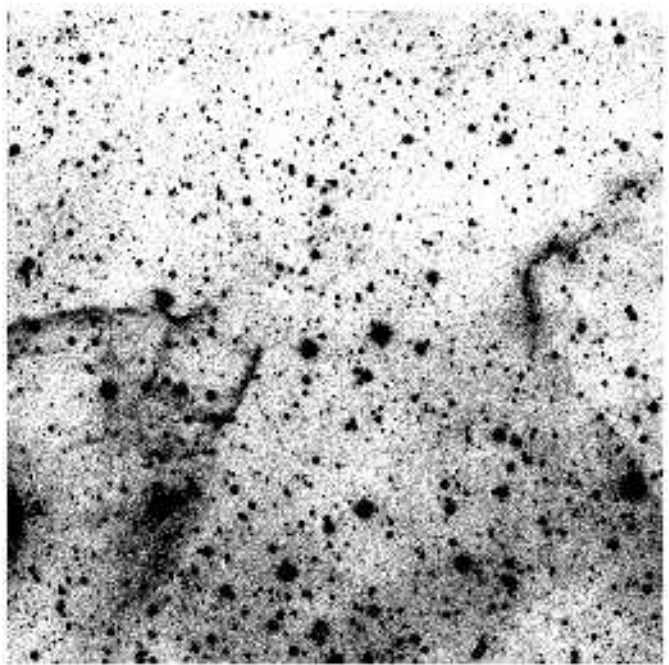


Fig. 2. $H\alpha$ image centered at northwest of HR Car. The field of view is $6'.75 \times 6'.75$. North is up and east is to the left. HR Car is visible at the southeastern edge of the frame.

tral $60'' \times 60''$ of the resultant $H\alpha$ image is displayed in Fig. 3. The y filter and the $H\alpha$ filter have quite a large difference in their central wavelengths. Thus stars with extreme red or blue colors will be either under- or over-subtracted, and appear dark or white in Fig. 3. The white arc to the north of HR Car is caused by an over-subtraction of the continuum caused by a low-intensity ghost in the y-filter images.

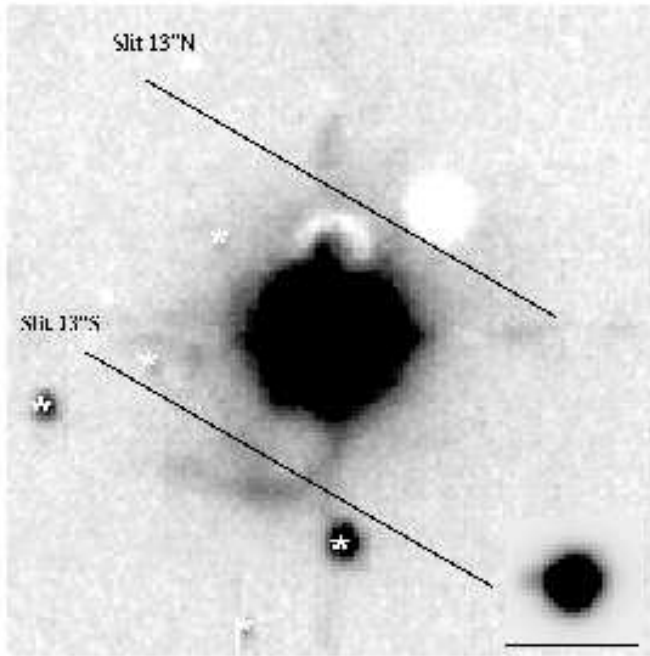


Fig. 3. $H\alpha$ image of the nebula around HR Car. The field of view is $60''$ by $60''$. North is up and east is to the left. The continuum is subtracted to our best effort. The over- and under-subtracted stars are the effect of their extreme colors. HR Car has a strong stellar $H\alpha$ emission and hence remains bright in the continuum-subtracted image. The inset at the lower right corner shows HR Car and its visual companion at the same plate scale as the main image in this figure.

2.2. Echelle spectroscopy

We obtained high-dispersion spectroscopic observations of the nebula around HR Carinae with the echelle spectrograph on the 4 m telescope at Cerro Tololo Inter-American Observatory in January 1996. We used the long-slit mode, inserting a post-slit $H\alpha$ filter ($6563/75 \text{ \AA}$) and replacing the cross-disperser with a flat mirror. A 791 mm^{-1} echelle grating was used. The data were recorded with the long focus red camera and the 2048×2048 Tek2K4 CCD. The pixel size was $0.08 \text{ \AA pixel}^{-1}$ along the dispersion, and $0''.26 \text{ pixel}^{-1}$ perpendicular to the dispersion. The slit length was effectively limited by vignetting to $\sim 4'$. Both $H\alpha$ 6563 \AA and the $[\text{N II}]$ 6548 \AA , 6583 \AA lines were covered

in the setup. The slit-width was $250 \mu\text{m}$ ($\cong 1''.64$) and the instrumental FWHM was about 14 km s^{-1} at the $H\alpha$ line. The seeing was $\sim 2''$ during the observations. Thorium-Argon comparison lamp frames were taken for wavelength calibration and geometric distortion correction.

Two slit positions were observed. One was offset by $13''$ to the north of HR Car, and the other $13''$ to the south of HR Car. For both positions the slit was rotated to a position angle of $\text{PA} = 60^\circ$. The slit positions are marked in Fig. 3. The exposure time was 600 s for the $13''$ S position and 300 s for the $13''$ N position. The echelle images of the $H\alpha + [\text{N II}]$ lines are presented in Fig. 4. Unfortunately, the echelle observations were made before our discovery of the funnel-shaped nebulosity to the northeast of HR Car, so no echelle observations of this nebulosity are available.

3. The bipolar nebula of HR Car

The nebula around HR Car has been classified as “filamentary nebula” by Nota et al. (1995) although a bipolar structure is suggested in Clampin et al.’s (1995) coronographic image, the best image of HR Car available in literature. In this coronographic image, the HR Car nebula appears elongated along the position angle $\sim 150^\circ$, with a size of approximately $37'' \times 19''$. The southeast lobe is brighter; it consists of a few nebular knots surrounded by a circular arc extending to $19''$ from the star. The northwest lobe is fainter and less well-defined.

Our images of the HR Car nebula do not have as high a resolution as the coronographic image, but our images are not occulted by a bar and the stars are not saturated. Using the Strömgren y images, we identified stars near HR Car and marked the stars in Fig. 3 with asterisks. We confirm the visual companion at $3''.5$ east of HR Car reported by Hutsemékers & Van Drom (1991). This visual companion is about 6^{m} fainter than HR Car. A y-band image of the HR Car and its companion is shown as an inset in Fig. 3.

Some of the non-stellar emission features along the refraction spikes are probably unreal, but the remaining diffuse emission features are real and belong to the bipolar nebula of HR Car. The polar axis measured from the central star and the southeast lobe is at $\text{PA} = 125 \pm 5^\circ$. The discrepancy of 25° between this measurement and that measured from the coronographic image is caused by the occulting bar which occulted the northern rim of the southeast lobe in the coronographic image. The size of the southeast lobe measured from our images is $19''$ along the polar axis and $24''$ perpendicular to the polar axis. The northwest lobe is faint; only the east rim of this lobe is easily seen in Fig. 3.

4. Kinematics of the HR Car nebula

The long-slit echelle data were used to study the physical structure of HR Car’s nebula and to determine the

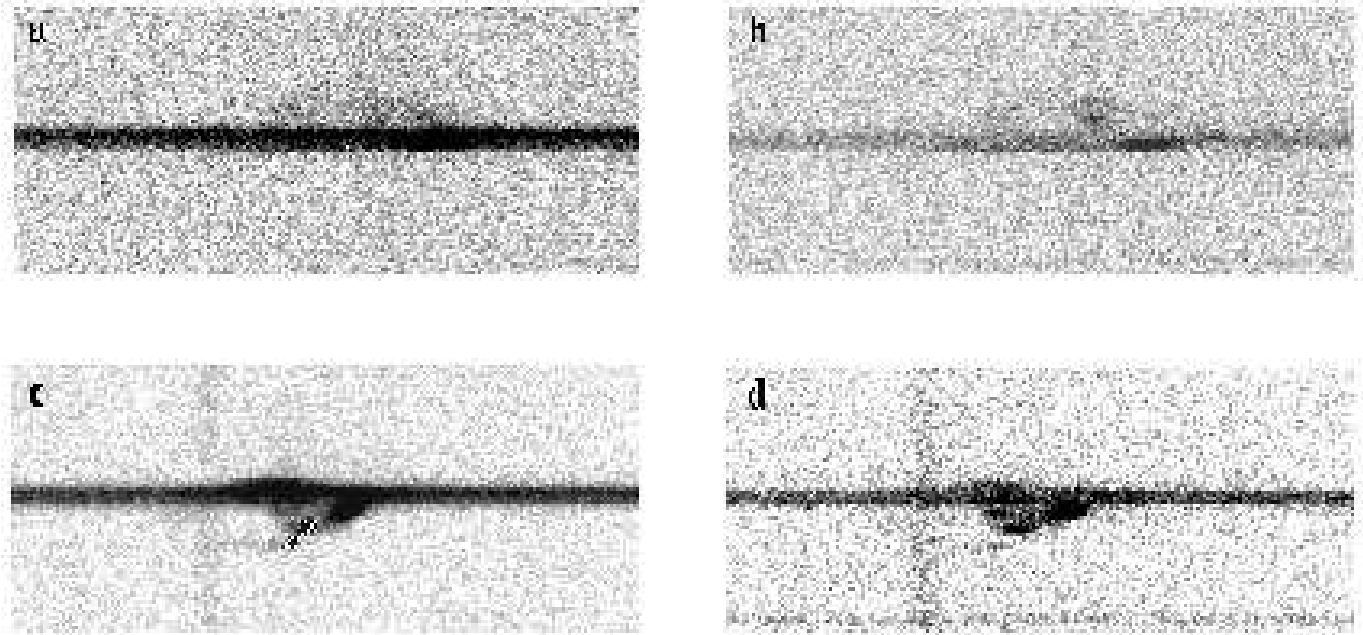


Fig. 4. Echellograms of the HR Car nebula: (a) the $H\alpha$ line of the northwestern lobe, (b) the $[N II] \lambda 6583$ line of the northwestern lobe, (c) the $H\alpha$ line of the southeastern lobe, and (d) the $[N II] \lambda 6583$ line of the southeastern lobe. The horizontal axis is the position along the slit and covers $78''$. Northeast is to the left and southwest is to the right. The vertical axis is along the spectral dispersion and covers 13 \AA , or 600 km s^{-1} . The wavelength (or velocity) increases upward. The background $H II$ component has $v_{LSR} = -10.6 \text{ km s}^{-1}$.

radial velocities of the nebula and its background $H II$ region. The brightest feature in the echelle images of the $H\alpha$ and $[N II]$ lines is the extended background component at nearly constant velocity $v_{LSR} = -10.6 \pm 2 \text{ km s}^{-1}$. The $[N II] \lambda 6583 \text{ \AA} / H\alpha$ ratio of the background component is $0.30 - 0.35$, which is quite common for Galactic $H II$ regions (Shaver et al. 1983).

The echelle images reveal two kinematic components in the HR Car nebula (Fig. 4). One component has a contiguous expansion structure and corresponds to the circular filaments, or the lobes. The other component consists of knots expanding at slower velocities and corresponds to the knots encompassed by the circular filaments. The expanding lobe component has $[N II] \lambda 6583 \text{ \AA} / H\alpha$ ratios of 0.30 ± 0.05 , similar to those in the background $H II$ component, while the knots have $[N II] \lambda 6583 \text{ \AA} / H\alpha$ ratios approaching 0.9, much higher than those in the lobes or the background $H II$. Hutsemékers & Van Drom (1991) obtained a $[N II] \lambda 6583 \text{ \AA} / H\alpha$ ratio of 0.43, which may reflect a mixture of emission from lobe and knot components in their aperture.

The two kinematic components of the HR Car nebula are individually discussed below.

4.1. The expanding lobes

We have measured the radial velocities in $H\alpha$ and the $[N II] \lambda 6583 \text{ \AA}$ lines, and plotted them against positions

along the slit in Fig. 5. The origin of the position-axis is where the slit intersects the polar axis ($PA = 150^\circ$, as measured from the coronagraphic image). Offsets are positive to the southwest and negative to the northeast. For reference, a dashed line is drawn at the velocity of the background emission, $v_{LSR} = -10.6 \text{ km s}^{-1}$.

Comparisons between the continuum-subtracted $H\alpha$ image (Fig. 3) and the echelle line images (Fig. 4) indicate that the filamentary structure seen in the $H\alpha$ image is connected through a faint expanding shell. The circular filament extending to $19''$ southeast of HR Car corresponds to the rim of the expanding shell, or lobe. The higher surface brightness of the circular filament is caused by the larger emitting depth along the line of sight. The echelle images also reveal that the bipolar lobes of HR Car are larger than what we measured in our continuum-subtracted $H\alpha$ image (Fig. 3).

The echelle slit positions were selected in assumption that the polar axis was along $PA = 150^\circ$. Fig. 5 shows that the largest expansion velocity along the northern slit position occurs at about $5''$ southwest of the assumed polar axis, and that along the southern position occurs at about $5''$ northeast of the assumed polar axis. This position difference indicates that the position angle of the polar axis should be smaller than $PA = 150^\circ$, supporting the $PA = 125^\circ \pm 5^\circ$ measurement made with our $H\alpha$ images.

The velocity structure of the two lobes is typical for a bipolar expansion. The northwestern lobe shows the largest receding velocity at $v_{\text{LSR}} = +92 \pm 8 \text{ km s}^{-1}$ and the largest approaching velocity at $v_{\text{LSR}} = -48 \pm 8 \text{ km s}^{-1}$, while the southeastern lobe shows the largest approaching velocity at $v_{\text{LSR}} = -133 \pm 8 \text{ km s}^{-1}$ and the largest receding velocity at $v_{\text{LSR}} = +30 \pm 8 \text{ km s}^{-1}$. If we assume point symmetry with respect to the star, these four extreme velocities can be averaged algebraically to determine the systemic velocity of the nebula, $\sim -14 \pm 5 \text{ km s}^{-1}$. The interpretation or modeling of the velocity structure observed in the lobes is complicated by three factors: (1) the lobes are not spherically symmetric, (2) the velocity vectors are not necessarily perpendicular to the lobe surface, and (3) the inclination angle of the polar axis is unknown. Given the limited amount of echelle data, we can conclude that both lobes are expanding, but more observations are needed for further modeling of the expansion. Note that the approaching side of the southeast lobe may have different velocities in the $\text{H}\alpha$ and $[\text{N II}]$ lines. Unfortunately, our data do not have adequate S/N ratios to analyze this result further.

The systemic velocity of the nebula around HR Car is close to the background H II velocity at -10.6 km s^{-1} , but very different from the LSR-velocity of $+9 \text{ km s}^{-1}$ reported by Hutsemékers & Van Drom (1991). Nevertheless our radial velocity is within the range of velocities measured by them for different ions in the stellar spectrum. The kinematic distance implied by our systematic velocity of $v_{\text{LSR}} = -14 \text{ km s}^{-1}$ is $2.3 \pm 0.5 \text{ kpc}$. Since peculiar velocities can affect the kinematic distance, we will adopt the 5 kpc.

The background H II velocity is very similar to the velocity of the Carina nebula (Courtès et al. 1966; Walborn & Hesser 1975). This may be related to the position of HR Car projected onto a faint, outer arc of the Carina nebula. The complex Na I interstellar absorption line profile as discussed by Hutsemékers & Van Drom (1991) with its components between $+9$ and -99 km s^{-1} can then be naturally explained by the motions inside the Carina H II complex (Walborn et al. 1984).

4.2. $[\text{N II}]$ -bright knots

Beside the main expansion structure, several $[\text{N II}]$ -bright knots were detected in the echelle data. We have identified 5 knots, 4 along the south slit and 1 along the north slit. These knots are plotted as small squares in Fig. 5. Their velocities (see Table 1) scatter between -75 km s^{-1} and $+34 \text{ km s}^{-1}$, always slower than the superimposed expanding lobe component. These knots can be identified in the $\text{H}\alpha$ image in Fig. 3. All of these knots are inside or close to the bipolar main structure.

Knots #1 – #4 are located in the southeastern lobe. Knots #1 and #2 are projected near the center of the southeastern lobe and they expand slower than the

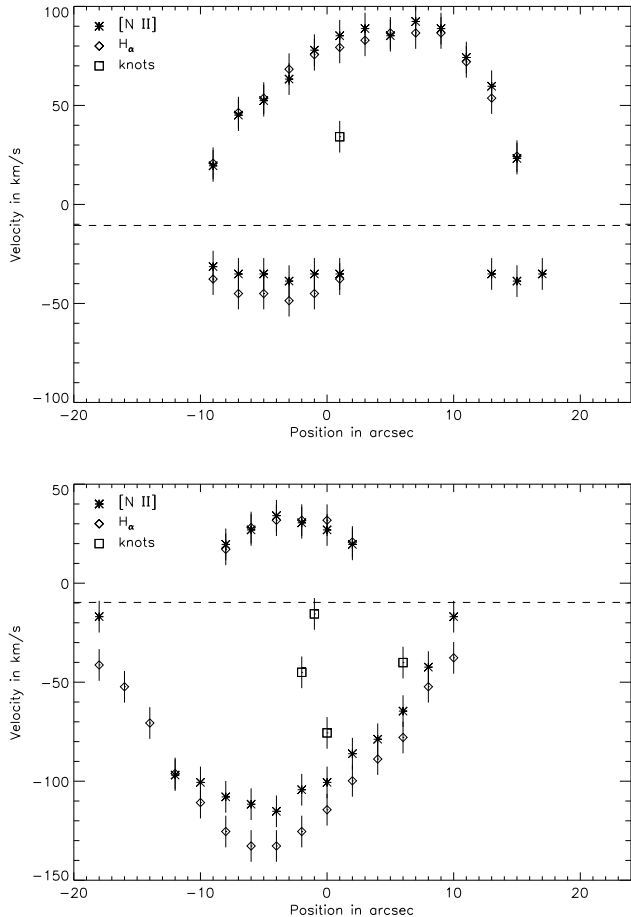


Fig. 5. Velocity-position plots of the northern slit position (top) and the southern slit position (bottom). Velocities are in LSR system. The origin of the position-axis is at $9'8$ north and $5'6$ west of HR Car in the top plot, and $9'8$ south and $5'6$ east of HR Car in the bottom plot. The slit is oriented along $\text{PA} = 60^\circ$. The offsets are positive to the southwest and negative to the northeast.

lobe. The different expansion velocities and the different $[\text{N II}]\lambda 6583 \text{ \AA}/\text{H}\alpha$ ratios indicate that these knots could not have the same origin as the expanding lobe. It is not known whether the knots are physically inside the lobes or are only projected within. Knots #3 and #4 follow roughly the expansion of the lobe, but a few km s^{-1} slower than the lobe. The similarities in expansion velocity and projected position may be suggestive of physical interaction between the knots and the expanding lobe.

Knot #5 is projected within the northwestern lobe. Like Knots #1 and #2, Knot #5 has an intermediate velocity that is slower than the expansion of the lobe. There is possibly another knot on the approaching side of the northwestern lobe. Kinematically it is not very different from the lobe, but the $[\text{N II}]\lambda 6583 \text{ \AA}/\text{H}\alpha$ ratio is higher, ~ 0.6 .

High $[\text{N II}]\lambda 6583 \text{ \AA}/\text{H}\alpha$ ratios in LBV nebulae or knots are quite common. For example, the $[\text{N II}]\lambda 6583 \text{ \AA}/\text{H}\alpha$ ratio for the S condensation of η Car nebula maybe as high as a $\simeq 7.5$ (Davidson et al. 1982). For AG Car, de Freitas Pacheco et al. (1992) found a value of $[\text{N II}]\lambda 6583 \text{ \AA}/\text{H}\alpha = 0.48 \pm 0.05$.

Similar $[\text{N II}]$ -bright knots have been observed in ring nebulae around Wolf-Rayet stars (e.g., RCW 104, Goudis et al. 1988), but their origin is unknown. These knots are also reminiscent of the FLIERS seen in planetary nebulae, which have been suggested to be high-density, collimated material expelled recently from the nucleus (Balick et al. 1994). A high nitrogen abundance has been derived for $[\text{N II}]$ -bright Wolf-Rayet nebulae (M1-67, Esteban et al. 1991; NGC 6888, Esteban & Vílchez 1992), as well as $[\text{N II}]$ -bright knots in planetary nebulae (NGC 6571, Chu et al. 1991). It is very likely that the $[\text{N II}]$ -bright knots in the HR Car nebula are overabundant in nitrogen. The nitrogen enhancement fits well to the interpretation of HR Car being an LBV which lost processed material via outbursts. The overabundance of nitrogen follows naturally from the ongoing CNO cycle in the star, confirming LBVs to be evolved stars (Maeder 1983; Langer et al. 1994).

Table 1. Positions and velocities of the $[\text{N II}]$ -bright knots.

knot #	lobe and position	velocity km s^{-1}	$[\text{N II}]\lambda 6583 \text{ \AA}/\text{H}\alpha$
1	southeast $-2''$	-45.1	0.88
2	southeast $-1''$	-15.5	0.88
3	southeast $0''$	-75.6	*
4	southeast $6''$	-40.1	0.83
5	northwest $1''$	$+34.2$	0.90

* The $\text{H}\alpha$ line was affected by a cosmic ray hit, and cannot be measured to give $[\text{N II}]\lambda 6583 \text{ \AA}/\text{H}\alpha$ ratio.

5. Structure and environment

We conclude that the nebula of HR Car is of bipolar structure and assume that the radial expansion velocity is no larger than the full velocity split and no smaller than 1/2 of the velocity split, or $75 \text{ km s}^{-1} < v_{\text{exp}} < 150 \text{ km s}^{-1}$. The northwestern and southeastern lobes have angular sizes of $26''$ and $28''$ along the slit, respectively. For a distance of 5 kpc, the linear sizes would be 0.63 and 0.67 pc. Assuming no additional acceleration, a lower limit on the dynamic age of the bipolar nebula is 4200 – 8400 yr.

The bipolar nebula of HR Car show intriguing similarities with the bipolar *Homunculus* nebula around the famous LBV η Car. At a distance of 2.5 kpc, each lobe of the Homunculus has a diameter of ~ 0.1 pc. This is a factor of 6 smaller than the lobes of HR Car. Therefore, it

is very likely that the nebula around HR Car is an older version of the Homunculus around η Car.

The gaseous environment of HR Car can be seen in the $\text{H}\alpha$ images in Figs. 1 and 2. A large funnel-shaped nebula is visible to the northwest of HR Car. This nebula is very faint. Only the brightest parts are barely visible on the ESO R plate in the Southern Sky Atlas. The axis of the funnel is roughly aligned with the the polar axis of the bipolar nebula around HR Car. This morphology suggests that HR Car is responsible for the ionization and shaping of this nebula.

Is this funnel-shaped nebula ejected by HR Car or an interstellar bubble blown by HR Car? At a distance of 5 kpc, the large shell structure would be located at 3 to 4.5 pc from HR Car. The ejecta of an LBV would need 26000 years to reach this distance from the star (assuming $v_{\text{exp}} = 150 \text{ km s}^{-1}$). This time interval is comparable to the lifetime of the LBV phase. Assuming $v_{\text{exp}} = 240 \text{ km s}^{-1}$, a typical intermediate velocity of the shell from a LBV ejecta (García-Segura et al. 1996), the filament at around 4 pc would be reached within 16000 yr. This would imply the possibility that this structure could be a remnant of an older ejecta from HR Car. If so, HR Car may be an already older LBV, which is consistent with its position in the HR diagram. An older age is implied by HR Car’s being situated significantly beneath the Humphreys-Davidson limit (Humphreys & Davidson 1994).

Another possible scenario to connect this outer nebulosity with HR Car is to identify it as a wind-blown bubble. Fast stellar wind of massive stars in their main-sequence phase will sweep up ambient medium and form “interstellar bubbles” (Weaver et al. 1977). The dynamic age of such a bubble is $\eta(R/v_{\text{exp}})$, with R being the bubble radius and v_{exp} its expansion velocity. The parameter η is 0.6 for an energy-conserving bubble in a homogeneous medium (Weaver et al. 1977) or 0.5 for a momentum-conserving bubble (Steigman et al. 1975). Assuming a typical wind-blown bubble expansion velocity of 20 km s^{-1} , the dynamical age of this bubble (with the northern filaments being its border) would be between 1 and 2×10^5 yr. With HR Car being already in the LBV phase a wind-blown bubble created in the main sequence state must be older than the 10^5 yr we find. If the northwestern nebulosity is connected to HR Car a wind-blown bubble scenario is not likely.

A net-like internal structure of this feature can very well be seen in Fig.2, fitting to the scenario of an expanding shell structure. We note that as seen in Fig. 2 this nebulosity shows an additional $2'$ e.g. 2.9 pc long feature reaching towards the north-west. One may link this elongated cone to a blow out structure. To prove this and explain the origin of the north-western filamentary nebula further spectroscopic and kinematic investigations are needed.

Our echelle observations detect a background $\text{H}\alpha$ emission over the entire slit length ($\sim 4'$) at both slit positions. The velocity of this gas is $v_{\text{LSR}} \sim -10.6 \text{ km s}^{-1}$ (see Fig.

4 and Fig. 5, the dashed line). This background H II component has a velocity FWHM of 41 km s^{-1} (after removing the instrumental broadening of FWHM of 14 km s^{-1}). This velocity width, higher than the thermal broadening for a 10^4 K gas, indicates gas motion; however, there is no evidence for an expanding shell, since no line-split is observed. This could be caused by the presence of multiple unresolved velocity components or a large turbulence. As discussed in 4.1 this may be due to gas in the Carina H II Complex that is in line of sight to HR Car, or indicates extended diffuse local emission around HR Car.

6. Summary and Remarks

Using imaging data and high-dispersion spectroscopic data, we have analyzed the nebula around the LBV HR Car and confirmed its bipolar structure. The two lobes have angular sizes of approximately $26''$ and $28''$ and their expansion velocities amount to $75 - 150 \text{ km s}^{-1}$. Bipolar nebulae are actually not very common among the known LBVNs (Nota et al. 1995). The HR Car nebula will be the second bipolar LBVN ever reported, with the Homunculus Nebula of η Car being the first. The formation of the bipolar nebula around HR Car is probably similar to that of the Homunculus nebula. The Homunculus was ejected in the last century with an expansion velocity of $\simeq 700 \text{ km s}^{-1}$ (e.g., Gaviola 1950; Meaburn et al. 1987; Meaburn et al. 1993; Daminieli Neto et al. 1993). The LBV nebulae around HR Car and η Car provide an opportunity to probe the evolution of LBVNs. In such a scenario the formation of a LBVN starts with a nebula that looks more like the Homunculus (150 yr old) and then evolves into a structure similar to the bipolar nebula of HR Car (4000 – 9000 yr old). The formation and evolution of a LBVN may depend on the strength of the eruption, initial expansion velocity, and the mass and density in the shell as well as in the surrounding medium. Since so many parameters are unknown, it is necessary to identify and use as many LBVNs as possible to complete our understanding of LBVN formation and evolution.

Both LBVNs of HR Car and η Car show bipolar morphology pinched by an equatorial plane. This morphology may be supportive of the recent theory of wind compressed disks (Bjorkman and Cassinelli 1993; Mac Low et al. 1996). In these models, the disk of higher density in the equatorial plan, formed by the wind and rotation of the star during the main sequence phase, is responsible for the mass ejection in preferred polar directions, which lead to the formation of bipolar shaped LBVNs. To verify this formation mechanism, a better understanding of the kinematic structure of LBVN is needed.

Acknowledgements. KW thanks Mordecai Mac Low, Guillermo García-Segura, and Norbert Langer for stimulating discussions. We thank the referee, Damien Hutsemékers, for his comments and suggestions. DJB acknowledges support from the Alexander

von Humboldt Foundation through their Feodor Lynen Fellowship program. MDJ thanks the Brigham Young University Department of Physics and Astronomy for continued support of his research at CTIO. We thank Peter W. A. Roming for work done during the initial inspection of the optical imaging data, Richard Auer and Lisa Joner for editorial comments.

References

- Balick B., Perinotta M., Maccioni A., Terzian Y., Hajian A., 1994, ApJ 424, 800
 Bjorkman J.E., Cassinelli J.P., 1993, ApJ 409, 429
 Carlson E.D., Henize K.G., 1979, Vistas Astron. 23, 213
 Chu Y.-H., Manchado A., Jacoby G. H., Kwitter K. B., 1991, ApJ 376, 150
 Clampin M., Schulte-Ladbeck R.E., Nota A. et al., 1995, AJ 110, 251
 Courtés G., Cruvellier P., Georgelin Y., Astier N., 1966, J. Observateurs 49, 329
 Daminieli Neto A., Viotti R., Baratta G.B., de Araujo F.X., 1993, A&A 268, 183
 Davidson K., Walborn N.R., Gull T.R., 1982, ApJ 254, L51
 de Freitas Pacheco J.A., Daminieli Neto A., Costa R.D.D., Viotti R., 1992, A&A 266, 360
 Esteban C., Vílchez J. M., 1992, ApJ 390, 536
 Esteban C., Vílchez J. M., Smith L. J., Manchado A., 1991, A&A 244, 205
 García-Segura G., Mac Low M.-M., Langer N., 1996, A&A 305, 229
 Gaviola E., 1950, ApJ 111, 408
 Goudis C. D., Meaburn J., Whitehead M. J., 1988, A&A 191, 341
 Humphreys R. M., Davidson K., 1979, ApJ 232, 409
 Humphreys R. M., Davidson K., 1994, PASP 106, 1025
 Hutsemékers D., 1994, A&A 281, L81
 Hutsemékers D., Van Drom E., 1991, A&A 248, 141
 Langer N., Hamann W.-R., Lennon M. et al., 1994, A&A 290, 819
 Mac Low M.-M., Langer N., García-Segura G., 1996, BAAS 28, 38.6
 Maeder A., 1983, A&A 120, 113
 Meaburn J., Wolstencroft R.D., Walsh J.R., 1987, A&A 181, 333
 Meaburn J., Walsh J.R., Wolstencroft R.D., 1993, A&A 268, 283
 Nota A., Livio M., Clampin M., 1995, ApJ 448, 788
 Polcaro V.F., Viotti R., 1993, A&A 274, 807
 Shaver P.A., McGee R.X., Newton L.M., Danks A.C., Pottasch S.R., 1983, MNRAS 204, 53
 Steigman G., Strittmatter P.A., Williams R.E., 1975, ApJ 198, 575
 van Genderen A.M., Robijn F.H.A., van Esch B.P.M., Lamers H.J.G.L.M., 1991, A&A 246, 407
 Viotti R., 1995, Rev.Mex.Astron.Astrofis. SdC 2, 1
 Walborn N.R., Hesser J.E., 1975, ApJ 199, 535
 Walborn N.R., Heckathorn J.N., Hesser J.E., 1984, ApJ 276, 524
 Weaver R., McCray R.A., Castor J., Shapiro P., Moore R., 1977, ApJ 218, 377
 This article was processed by the author using Springer-Verlag L^AT_EX A&A style file L-AA version 3.